

Quantum Dynamical Simulation of Electron-Transfer Reactions in an Anharmonic Environment[†]

Haobin Wang

Department of Chemistry and Biochemistry, MSC 3C, New Mexico State University,
Las Cruces, New Mexico 88003

Michael Thoss*

Department of Chemistry, Technical University of Munich, 85748 Garching, Germany

Received: March 26, 2007; In Final Form: May 25, 2007

The multilayer multiconfiguration time-dependent Hartree theory is applied to study the quantum dynamics of ultrafast electron-transfer reactions in a condensed-phase environment with anharmonic potential functions. Effects of anharmonicity for both the nuclear degrees of freedom of the environment and the intramolecular vibrational degrees of freedom are investigated. Whereas the former can in principle be mapped to a fictitious harmonic bath, the latter cannot be represented in this way and, thus, go beyond the commonly employed linear response approximation. Numerical examples are presented to illustrate these findings.

I. Introduction

The accurate description of quantum effects for large molecular systems is a challenging task in theoretical chemical dynamics. Due to the rapid development in time-resolved nonlinear spectroscopy techniques, more detailed information on the reaction dynamics of complex molecular systems has become available in recent years. As a consequence, it has been realized that in many complex processes, quantum tunneling and coherence effects may play important roles. Such effects cannot be described by purely classical methods, such as, for example, molecular dynamics simulation. This has stimulated the development of theoretical methods that are capable of describing the quantum dynamics in systems with many degrees of freedom. According to their different nature, these methods can be broadly divided into two major classes: rigorous quantum dynamical methods and semiclassical approaches. The multi-configuration time-dependent Hartree (MCTDH) theory^{1–4} and, in particular, its multilayer (ML) generalization, the ML-MCTDH theory,⁵ are promising examples of the former class.

The feasibility of the MCTDH method has been demonstrated by many applications to gas-phase reactions of relatively large molecules.^{6–12} For reactions in a condensed-phase environment, there is currently no universal rigorous method available that is capable of simulating the quantum dynamics for a general complex molecular system with arbitrary potential functions. However, the MCTDH method has been proven extremely useful for treating certain classes of quantum dynamical processes in large molecular systems in a numerically exact way, in which a moderate number of degrees of freedom has been explicitly included in the dynamical treatment.^{13–17} An important example along this line is the system-bath Hamiltonian that models reactions in the condensed phase, for example, the spin–boson model^{18,19} for donor–acceptor electron transfer (ET) processes.²⁰ The MCTDH method, together with the self-consistent hybrid approach,^{14,21,22} has been shown to compare

favorably with the alternative path integral approach^{23–30} based on Feynman–Vernon influence–functional technique.³¹

The original MCTDH method is limited to treating a few tens of degrees of freedom. This is adequate for describing the dynamics of the spin–boson model in a relatively limited physical regime. To simulate quantum dissipative dynamics in a broader parameter space, the more versatile multilayer (ML) generalization of the MCTDH method has been proven useful.^{5,32–34} This is particularly important for treating donor–acceptor ET reactions in a complex condensed-phase environment in which both the intramolecular vibrational degrees of freedom of the donor–acceptor complex (inner sphere) and the continuous distribution of solvent modes (outer sphere) contribute to the overall vibronic dynamics.

In most previous studies of ET reactions in the condensed phase, the influence of the nuclear degrees of freedom is modeled by a bath of harmonic oscillators,^{19,20,35} which corresponds to a linear response model^{36,37} for the outer sphere solvent environment and a harmonic approximation for the inner sphere vibrational modes. This may be justified if the interaction of the donor–acceptor complex with the environment is evenly distributed over many nuclear degrees of freedom. There are, however, many situations in which this is not the case. Examples include strongly coupled low-frequency intramolecular modes (such as torsional motion) for which the harmonic approximation is not appropriate and ET in nonpolar liquids for which the linear response treatment may fail. Even in cases that the linear response approach is valid and, thus, a mapping to a fictitious harmonic bath is possible, it may be more convenient to simulate the quantum dynamics of the ET reaction in the original anharmonic environment. This is because such a mapping to a harmonic bath is temperature-dependent, which makes it difficult to systematically study the dependence of ET dynamics on various physical parameters (e.g., temperature, time scale, and coupling of the bath, etc.). From a theoretical perspective, it is also important to develop methods that can directly simulate ET reactions in an anharmonic environment. This not only

[†] Part of the special issue “Robert E. Wyatt Festschrift”.

generates benchmark results for developing other approximate theories that go beyond harmonic approximation^{38–41} but also provides a more general framework to test the validity of the linear response modeling procedure for treating ET reactions in the condensed phase.

The purpose of this paper is to study the effect of an anharmonic environment on ET reactions. A number of workers have studied the effect of anharmonicities in the intramolecular degrees of freedom on the ET reaction;^{38–43} however, so far, there have been only very few attempts to describe the quantum dynamics of reactions in an anharmonic environment based on path integral^{44–46} and semiclassical⁴⁷ methods. Here, we demonstrate the applicability of the ML-MCTDH method to simulate the quantum dynamics in such systems. The ML-MCTDH appears to be ideally suited to study such systems because, in contrast to the path integral method, the bath degrees of freedom are treated explicitly, and thus, the anharmonicity of the bath degrees of freedom makes little difference to the calculation.

The paper is organized as follows: Section II outlines the model employed in this paper, followed by a brief summary of the ML-MCTDH theory and some details of the calculation in Section III. Section IV presents the results of the dynamical simulations and discusses the connection to the linear response model. Finally, Section V concludes.

II. Model

To study ET reactions in a condensed-phase environment, we consider the generic Hamiltonian

$$H = H_s + H_b + H_{sb} \quad (2.1)$$

where H_s and H_b denote the Hamiltonian of the system and environment (the “bath”), respectively, and H_{sb} their interaction. In this paper, we employ a generalized spin–boson model in which the corresponding terms are given by

$$H_s = |\psi_1\rangle E_1 \langle \psi_1| + |\psi_2\rangle E_2 \langle \psi_2| + \Delta \sigma_x \quad (2.2a)$$

$$H_b = \sum_j \left[\frac{1}{2} p_j^2 + V_j(q_j) \right] \quad (2.2b)$$

$$H_{sb} = \sigma_z \sum_j W_j(q_j) \quad (2.2c)$$

Here, $|\psi_1\rangle$ and $|\psi_2\rangle$ denote the donor and acceptor state of the ET reaction, respectively, and σ_x and σ_z are Pauli matrices.

$$\sigma_x = |\psi_1\rangle \langle \psi_2| + |\psi_2\rangle \langle \psi_1| \quad (2.3a)$$

$$\sigma_z = |\psi_1\rangle \langle \psi_1| - |\psi_2\rangle \langle \psi_2| \quad (2.3b)$$

In all examples studied below, the electronic parameters for the system Hamiltonian are $E_1 = E_2 = 0$ (corresponding to a symmetric, for example, self-exchange, ET reaction) and $\Delta = 250 \text{ cm}^{-1}$.

Most quantum dynamical studies of ET processes in the condensed phase have been based on the spin–boson model. The spin–boson model corresponds to a harmonic approximation for $V_j(q_j)$ and a linear coupling term in $W_j(q_j)$.

$$V_j(q_j) = \frac{1}{2} \omega_j^2 q_j^2 \quad (2.4a)$$

$$W_j(q_j) = c_j q_j \quad (2.4b)$$

TABLE 1: Parameters of the Intramolecular Modes in the Model Hamiltonian (2.4) for the Spin–Boson Model, Including Vibrational Frequencies ω_j and Reorganization Energies λ_j of the Intramolecular Modes as well as the Electronic Free Energy Gap, $E_2 - E_1$, and Diabatic Coupling, Δ ^a

j	ω_j	λ_j	no. of basis functions
1	2100	250	8
2	650	250	12
3	400	250	16
4	150	250	24
$E_2 - E_1 = 0$		$\Delta = 250$	

^a All quantities are given in cm^{-1} . The last column specifies the number of primitive basis functions used in our simulations.

In this paper, the spin–boson model is used only for comparison with results for a more general anharmonic model (see below).

In the calculation presented below, we will consider models that include both a discrete set of intramolecular modes (inner sphere) and a continuous distribution of environment modes (outer sphere). The coupling of the intramolecular modes is usually specified by the reorganization energy, $\lambda_j = 2c_j^2/\omega_j^2$. In some of the examples discussed below, four intramolecular modes are included. Their frequencies and reorganization energies are given in Table 1.

The effect of the outer sphere bath is specified by its spectral density,¹⁹

$$J(\omega) = \frac{\pi}{2} \sum_j \frac{c_j^2}{\omega_j} \delta(\omega - \omega_j) \quad (2.5)$$

In this paper, we employ a bimodal form,

$$J_B(\omega) = J_G(\omega) + J_D(\omega) \quad (2.6)$$

with a Gaussian part accounting for the ultrafast inertial decay,

$$J_G(\omega) = \sqrt{\pi} \frac{\lambda_G \omega}{4\omega_G} e^{-[\omega/(2\omega_G)]^2} \quad (2.7a)$$

and a Debye part describing the slower diffusive decay,

$$J_D(\omega) = \frac{\lambda_D}{2} \frac{\omega \omega_D}{\omega^2 + \omega_D^2} \quad (2.7b)$$

The total reorganization energy of the ET reaction is given by $\lambda = \lambda_D + \lambda_G$. In the examples below, we use the following set of parameters: $\lambda_G = 250 \text{ cm}^{-1}$, $\omega_G = 200 \text{ cm}^{-1}$, $\lambda_D = 250 \text{ cm}^{-1}$, and $\omega_D = 20 \text{ cm}^{-1}$.

The solvent spectral density of eq 2.6 can be discretized to the form of eq 2.5 via the relation

$$c_j^2 = \frac{2}{\pi} \omega_j \frac{J_B(\omega_j)}{\rho(\omega_j)} \quad (2.8a)$$

where $\rho(\omega)$ is a density of frequencies satisfying

$$\int_0^{\omega_j} d\omega \rho(\omega) = j, \quad j = 1, \dots, N \quad (2.8b)$$

with N denoting the number of solvent modes in the simulation. The precise functional form of $\rho(\omega)$ does not affect the final answer if a sufficient number of modes are included. In this paper, we employ a simple discretization scheme in which the

frequencies are equally spaced. The density of frequencies is thus given by

$$\rho(\omega) = \frac{N}{\omega_m} \quad (2.9)$$

with $\omega_m = 800 \text{ cm}^{-1}$ the highest frequency considered. Although this discretization scheme is not as efficient as what we have used previously,^{14,21,22} it is more convenient for the purpose of comparing to results obtained with an anharmonic environment. For the examples presented in Seciton IV, we find that 50–150 bath modes are adequate to represent the bath continuum over the time scale of interest.

To study the effect of anharmonicity on the ET reaction, we consider a polynomial expansion of the bath potential $V_j(q_j)$ and the electronic–nuclear coupling $W_j(q_j)$ along each nuclear coordinate q_j up to the quartic order.

$$V_j(q_j) = \frac{A_j}{2}\omega_j^3 q_j^4 + \frac{B_j}{2}\omega_j^{5/2} q_j^3 + \frac{1}{2}\omega_j^2 q_j^2 + \frac{D_j}{2}\omega_j^{3/2} q_j \quad (2.10a)$$

$$W_j(q_j) = \frac{E_j}{2}\omega_j^3 q_j^4 + \frac{F_j}{2}\omega_j^{5/2} q_j^3 + \frac{G_j}{2}\omega_j^2 q_j^2 + c_j q_j \quad (2.10b)$$

The parameters ω_j , c_j of the original spin–boson model are determined from the spectral density as described above. In addition, in this model, there are six dimensionless parameters for each nuclear degree of freedom, A_j , B_j , D_j , E_j , F_j , and G_j , to describe anharmonic corrections to the standard harmonic bath model in eq 2.4. It is noted that the polynomial expansion in eq 2.10 neglects mode-mixing terms. The effect of such terms (e.g., Dushinski rotation⁵⁵) on the dynamics will be the subject of future work.

For the intramolecular modes, there is no fundamental restriction in choosing the anharmonicity parameters; they can be determined by fitting the potential energy surface along each q_j . For the infinite number of outer-sphere solvent modes, however, the Hamiltonian form in eq 2.2 requires that each coupling term in eq 2.10 follow a proper scaling versus the number of bath modes, N , to ensure that the correct thermodynamic limit is reached in the continuous limit.^{48,49} As discussed in ref 49, the dimensionless parameters in $W_j(q_j)$ generally need to scale as $1/N$ if all the terms are to be retained in eq 2.10. In this case, however, the bath has no direct dynamical influence on the system, and the effect of the environment is purely static, similar to static disorder. To discuss more interesting dynamics, we delete all odd power terms in V_j (i.e., $B_j = D_j = 0$) and all even power terms in W_j (i.e., $E_j = G_j = 0$). To reach the thermodynamic limit in the thus obtained model, it is required that the remaining coupling terms in W_j scale as $1/\sqrt{N}$.^{48,49} This requirement is naturally satisfied for c_j due to the definition of the spectral density (2.5) in the harmonic limit. For the cubic terms in W_j , it is required that F_j in eq 2.10 scale as $F_j = F/\sqrt{N}$, where F is a constant.

The observable of interest to study the dynamics of ET reactions is the time-dependent population of the donor state, given by

$$P(t) = \frac{1}{\text{tr}[e^{-\beta H_b}]} \text{tr}[e^{-\beta H_b} |\psi_1\rangle\langle\psi_1| e^{iHt} |\psi_1\rangle\langle\psi_1| e^{-iHt}] \quad (2.11)$$

Here, $\beta = 1/k_B T$, and we use atomic units (where $\hbar = 1$).

III. Dynamical Method

To simulate the quantum dynamics of the ET systems introduced above, we use the multilayer (ML) formulation⁵ of the multiconfiguration time-dependent Hartree (MCTDH) method^{1–4} in combination with an importance sampling scheme to describe the thermal initial condition in the observable (eq 2.11). The method as well as applications to different reactions in the condensed phase have been described in detail previously.^{5,32,50,51} Here, we only briefly introduce the general idea and give some details specific to the application in this work.

A. Multilayer Multiconfiguration Time-Dependent Hartree Theory. The ML-MCTDH method⁵ is a variational approach for the description of quantum dynamics in systems with many degrees of freedom. It extends the original MCTDH method^{1–4} for applications to significantly larger systems. In the original (single-layer) MCTDH method, the overall wave function is expanded in terms of time-dependent configurations.

$$|\Psi(t)\rangle = \sum_J A_J(t) |\Phi_J(t)\rangle \equiv \sum_{j_1} \sum_{j_2} \cdots \sum_{j_M} A_{j_1 j_2 \cdots j_M}(t) \times \prod_{k=1}^M |\phi_{j_k}^k(t)\rangle \quad (3.1)$$

Here, $|\phi_{j_k}^k(t)\rangle$ is the “single-particle” (SP) function for the k th SP degree of freedom, and M denotes the number of SP degrees of freedom. Each SP group usually contains several (Cartesian) degrees of freedom in our calculation, and for convenience, the SP functions within the same SP degree of freedom are chosen to be orthonormal.

In contrast to the original MCTDH method, in which the SP functions are represented by time-independent basis functions,

$$|\phi_n^k(t)\rangle = \sum_I B_I^{k,n}(t) |u_I^k\rangle \quad (3.2)$$

the ML-MCTDH method employs a *dynamic* contraction of the basis functions that constitute the SP functions. To this end, a *time-dependent* multiconfigurational expansion of the SP functions is used,

$$|\phi_n^k(t)\rangle = \sum_I B_I^{k,n}(t) |u_I^k(t)\rangle \equiv \sum_{i_1} \sum_{i_2} \cdots \sum_{i_{Q(k)}} B_{i_1 i_2 \cdots i_{Q(k)}}^{k,n}(t) \prod_{q=1}^{Q(k)} |v_{i_q}^{k,q}(t)\rangle \quad (3.3)$$

that is, the basic strategy of MCTDH is adopted to treat each SP function. Here, $Q(k)$ denotes the number of level two (L2)–SP degrees of freedom in the k th level one (L1)–SP group, and $|v_{i_q}^{k,q}(t)\rangle$ is the L2–SP function for the q th L2–SP degree of freedom. Employing two dynamical layers, the expansion of the overall wave function can thus be written in the form

$$|\Psi(t)\rangle = \sum_{j_1} \sum_{j_2} \cdots \sum_{j_M} A_{j_1 j_2 \cdots j_M}(t) \times \prod_{k=1}^M \left[\sum_{i_1} \sum_{i_2} \cdots \sum_{i_{Q(k)}} B_{i_1 i_2 \cdots i_{Q(k)}}^{k,j_k}(t) \prod_{q=1}^{Q(k)} |v_{i_q}^{k,q}(t)\rangle \right] \quad (3.4)$$

The extension to more dynamical layers is obvious. In the calculation considered below, two dynamical layers are employed.

The equations of motion within the ML-MCTDH approach can be obtained from the Dirac–Frenkel variational principle.⁵ For two layers, they are given by

$$i|\dot{\Psi}(t)\rangle_{L1 \text{ coefficients}} = \hat{H}(t)|\Psi(t)\rangle \quad (3.5a)$$

$$i|\dot{\phi}^k(t)\rangle_{L2 \text{ coefficients}} = [1 - \hat{P}^k(t)][\hat{\rho}^k(t)]^{-1}\langle \hat{H}(t) \rangle^k |\phi^k(t)\rangle \quad (3.5b)$$

$$i|\dot{v}^{k,q}(t)\rangle_{L3 \text{ coefficients}} = [1 - \hat{P}_{L2}^{k,q}(t)][\hat{\rho}^{k,q}(t)]^{-1}\langle \hat{\mathcal{H}}(t) \rangle^{k,q} |v^{k,q}(t)\rangle \quad (3.5c)$$

where the mean-field operators, reduced densities, and projection operators are defined in ref 5. The equations of motion for additional layers are again obvious extensions of eq 3.5. The inclusion of several dynamically optimized layers in the ML-MCTDH method provides more flexibility in the variational functional, which significantly advances the capabilities of performing wave packet propagations in complex system. This has been demonstrated by several applications to quantum dynamics in the condensed phase, including many degrees of freedom.^{5,32–34,50,52,53}

B. Details of the Calculation. The ML-MCTDH theory outlined above is applied to simulating quantum dynamics of the model Hamiltonian in eq 2.2, where both harmonic and anharmonic model potentials have been treated. The results are obtained with two upper dynamic layers and one deeper static layer, which we generally refer to as the two-layer version of the ML-MCTDH. To evaluate the trace in eq 2.11, a Monte Carlo average is carried out employing an importance sampling technique according to the weighting function provided by the Boltzmann operator.^{5,14,22} Thereby, depending on the specific parameters, hundreds to thousands of statistical samples are required to achieve convergence.

For the examples considered below, one level 1 (L1) SP group is assigned for the intramolecular modes (if they are present) and another four L1-SP groups are assigned for the solvent modes. The number of level 2 (L2) SP groups varies between two and six for different L1-SP groups. In the third static layer, up to six Cartesian degrees of freedom are contained in each SP group. The basis functions for the spin–boson model of eq 2.4 are naturally chosen as eigenfunctions of each harmonic mode. For the anharmonic model in eq 2.10, they are chosen as eigenfunctions of $p_j^2/2 + V_j$ for each quartic degree of freedom. This is done by using primitive basis functions of harmonic oscillator eigenfunctions to express V_j and W_j and diagonalizing $p_j^2/2 + V_j$ to obtain its eigenfunctions. A corresponding transformation is then made to express W_j in terms of this basis set. Afterward, a sufficient number of basis functions is employed for each degree of freedom based on both the temperature (such that the highest state has negligible Boltzmann weighting) and the coupling strength to the electronic states. This number is listed in Table 1 for the intramolecular modes. For outer-sphere solvent modes, it varies from 5 to 130, depending on the frequency and the anharmonicity of the modes, although a smaller number of basis functions may also give the correct result. Finally, the basis functions of the static layer are adiabatically contracted, as done previously.^{5,14,22}

An important factor to obtain numerically exact results within the ML-MCTDH approach is to use enough time-dependent configurations for each layer. This is achieved by converging the number of SP functions for each SP degree of freedom in repeated test calculations. For the examples discussed in this paper, a relatively large number of SP functions for the groups of the intramolecular modes is needed to achieve convergence:

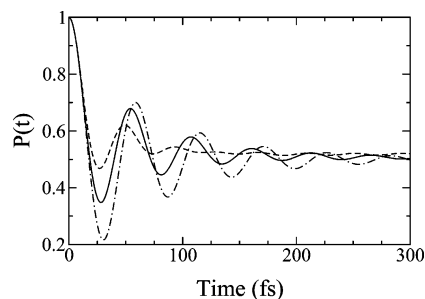


Figure 1. Time-dependent population of the donor electronic state for the generalized spin–boson model, eq 2.2, at $T = 300$ K. The parameters for the electronic states and the bath are given in Section 1. The anharmonic parameters in eq 2.10 are defined as pure harmonic bath (—); $A_j = 0.2$ for all bath modes and zero for all other parameters (– · – ·); $F_j = 0.2/\sqrt{N}$ for all bath modes and zero for all other parameters (– –).

20–40 for the L1-SP group and 16–28 for the L2-SP groups. Comparably, this number is smaller for the solvent SP groups: 8–10 for the L1-SP groups and 4–6 for the L2-SP groups. The resulting total configurational space is 2000–720 000 for the first layer and 600–15 000 for each second layer, where the larger configuration space is required when strongly coupled intramolecular modes are included in the model. The CPU cost for one wave function thus varies significantly, ranging from a few minutes to as many as 20 h on a 2.8 GHz Pentium 4 PC (the more expensive ones are used mainly to ensure that full convergence is reached.) Depending on the temperature, up to a few hundred Monte Carlo samples are sufficient to achieve statistical convergence when intramolecular modes are included in the model and a few thousand samples for models without them.

IV. Results

We first study the influence of an anharmonic environment on the ET reaction using models without intramolecular modes. As discussed in Section II, we include even power terms of V_j and odd power terms of W_j in eq 2.10. Furthermore, we require that the coupling constants in W_j (F_j , c_j) scale as $1/\sqrt{N}$ to ensure a proper thermodynamic limit. Figure 1 shows the time-dependent population of the donor state, $P(t)$, for the parameters given in Section II. Three cases are considered: the standard spin–boson model with a harmonic bath and linear electronic–nuclear coupling (solid line) and two generalized spin–boson models with an additional anharmonic term in either V_j (dashed-dotted line) or W_j (dashed line). For the parameter regime considered here, the ET dynamics is characterized by pronounced electronic coherence effects, which are quenched for longer times due to the interaction with the environment.

Compared with the harmonic bath model (solid line in Figure 1), the amplitude of the electronic oscillations increases when including the quartic term of the bath potential while retaining only the linear electronic–nuclear coupling (dashed-dotted line). This indicates that the quartic anharmonicity of the bath reduces the effective electronic–nuclear coupling. This can be rationalized by the fact that the energy levels of a quartic oscillator have a larger spacing than that of a harmonic oscillator, thus resulting in an effectively smaller density of states at lower energy. On the other hand, the electronic coherence effects are quenched when including an additional cubic term in W_j while retaining a harmonic bath (dashed line). This is due to the fact that the additional cubic term increases the effective electronic–nuclear coupling.

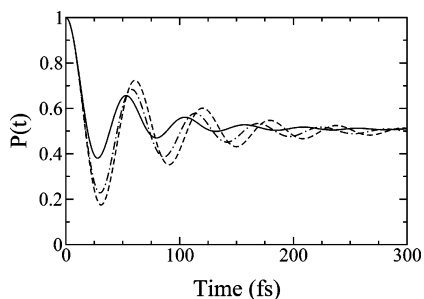


Figure 2. Time-dependent population of the donor electronic state for the generalized spin-boson model, eq 2.2, at $T = 300$ K. The anharmonic parameters in eq 2.10 are defined as $F_j = 0.05/\sqrt{N}$ for all bath modes and zero for all other parameters except $A_j = 0.0$ (—), $A_j = 0.2$ (— · —), and $A_j = 0.5$ (— —).

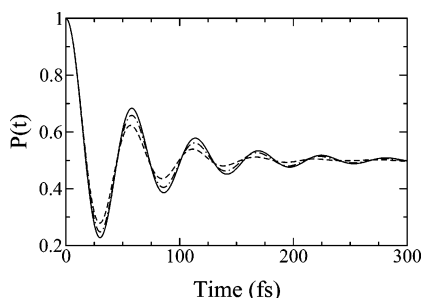


Figure 3. Time-dependent population of the donor electronic state for the generalized spin-boson model, eq 2.2, at $T = 300$ K. The anharmonic parameters in eq 2.10 are defined as $A_j = 0.2$ for all bath modes and zero for all other parameters except $F_j = 0.05/\sqrt{N}$ (—), $F_j = 0.1/\sqrt{N}$ (— · —), and $F_j = 0.2/\sqrt{N}$ (— —).

The two anharmonic models considered above differ from the standard harmonic bath spin-boson model only by either an additional quartic term or an additional cubic coupling. The general trend observed remains qualitatively the same, even when more complicated anharmonic models are used. This is demonstrated in Figures 2 and 3, which show results of the generalized spin-boson model in which anharmonic terms are included in both V_j and W_j . As illustrated in Figure 2, increasing the quartic anharmonic strength in V_j results in more pronounced electronic coherence in $P(t)$. The opposite trend is found for increasing the cubic anharmonic strength in W_j , as shown in Figure 3. These findings are consistent with those of simpler models in Figure 1.

At a particular temperature, the models of ET reactions in an anharmonic bath discussed above can, in principle, be mapped exactly to the spin-boson model with a fictitious harmonic bath. This is achieved by Fourier transforming the force-force autocorrelation function of the anharmonic bath,

$$C_{\beta}(t) = \frac{1}{\text{tr}[e^{-\beta H_b}]} \text{tr}[e^{-\beta H_b} \sum_j W_j(q_j) e^{iH_b t} \sum_j W_j(q_j) e^{-iH_b t}] \quad (4.1)$$

to give an effective, temperature-dependent spectral density³⁷

$$J_{\text{eff}}(\omega, \beta) = 2 \tanh\left(\frac{\beta\omega}{2}\right) \int_0^{\infty} dt \text{Re}[C_{\beta}(t)] \cos(\omega t) \quad (4.2)$$

It is noted that for the ET model considered here, the force-force autocorrelation function corresponds to the energy-gap correlation function.

Figure 4 shows the effective spectral density $J_{\text{eff}}(\omega, \beta)$ for different anharmonicity parameters. The spectral densities

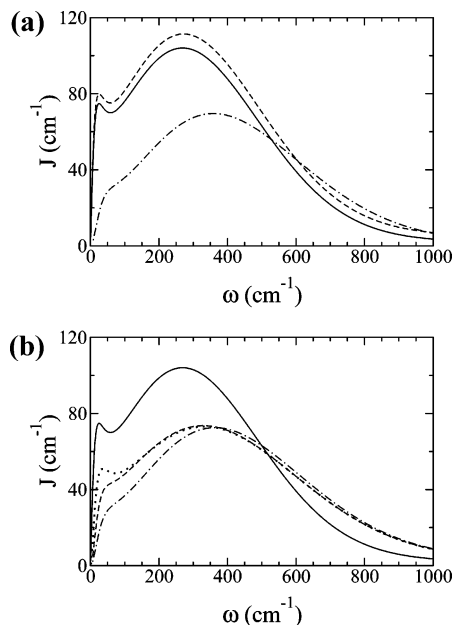


Figure 4. Effective spectral density obtained from eq 4.2 for the anharmonic models described in the text. (a) Models that correspond to Figure 1 at 300 K: original spectral density with the harmonic bath (—), $A_j = 0.2$ for all bath modes and zero for all other parameters (— · —); $F_j = 0.2/\sqrt{N}$ for all bath modes and zero for all other parameters (— —). (b) Dependence of the spectral density on the temperature for the anharmonic parameters $A_j = 0.2$ and $F_j = 0.2/\sqrt{N}$ for all the bath modes and zero otherwise: $T = 300$ K (— · —), $T = 100$ K (— —), $T = 25$ K (····). For comparison, the original spectral density with the harmonic bath is also shown (—).

depicted in panel (a) correspond to the dynamical results shown in Figure 1, representing models that include either a quartic anharmonicity (dashed-dotted line) or a cubic coupling term (dashed line). The comparison with the spectral density of the corresponding harmonic spin-boson model, $J(\omega)$, eq 2.6 (in which all anharmonic parameters have been set to zero) reveals that especially the quartic anharmonicity results in a significantly altered effective spectral density, $J_{\text{eff}}(\omega, \beta)$. In particular, the effective spectral density has smaller values than the corresponding harmonic spectral density for low frequencies and slightly larger values for higher frequencies. This is a consequence of the fact that effective spectral density describes a bath of quartic oscillators, the energy levels of which are shifted to higher energies with respect to those of the corresponding harmonic oscillators. Overall, the effective spectral density shows that in the model with the quartic bath, the electron-nuclear coupling is significantly smaller, which results in the more pronounced electronic coherence effects observed in the dynamical results in Figure 1. The additional cubic coupling term (without anharmonic potential), on the other hand, results in an almost frequency-independent, relatively small increase of the value of the spectral density. This corresponds to a larger electron-nuclear coupling, which results in a faster quenching of the electronic coherence, as observed in the dynamics of $P(t)$ in Figure 1.

The dependence of the effective spectral density on the temperature of the anharmonic bath is illustrated in Figure 4b. It is seen that a higher temperature results in an overall more structureless effective spectral density. Furthermore, the intensity of the low-frequency part of the effective spectral density decreases for higher temperature. The latter result is a consequence of the fact that for higher temperatures, the occupation shifts to states with higher energies.

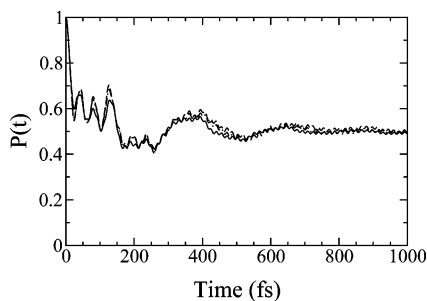


Figure 5. Time-dependent population of the donor electronic state for the generalized spin–boson model for which four intramolecular modes in Table 1 are included in addition to the outer-sphere bath. The anharmonic parameters in eq 2.10 are defined as $A_j = 0.2$ and $F_j = 0.2/\sqrt{N}$ for all outer-sphere bath modes. The intramolecular modes are harmonic with linear coupling to the electronic states. Three temperatures are shown: 300 (—), 100 (---), and 25 K (- - -).

The mapping of an anharmonic bath to a fictitious harmonic bath is possible within linear response theory if the coupling term $W_j(q_j)$ obeys the proper scaling ($\sim 1/\sqrt{N}$). This scaling is required for extended (nonlocal) nuclear modes to ensure that the thermodynamic limit is reached for an infinite number of nuclear degrees of freedom. However, it is not a necessary requirement that all nuclear degrees of freedom of an ET system in a condensed-phase environment follow this scaling law. An important example, which will be discussed below, is ET reactions involving strongly coupled anharmonic intramolecular degrees of freedom. Despite the fact that the force–force autocorrelation function for such systems can still be obtained theoretically or experimentally in this situation, a mapping to the harmonic bath spin–boson model may lead to serious errors. It is thus crucial to perform dynamical studies with the original anharmonic potential functions.

We next consider ET models that include the influence of intramolecular modes (inner sphere), of the donor–acceptor complex. Figure 5 shows $P(t)$ at 100 K for a model with four intramolecular modes, as listed in Table 1. The parameters for the electronic states and the outer-sphere bath are the same as discussed above. The anharmonic parameters in eq 2.10 are defined as $A_j = 0.2$ and $F_j = 0.2/\sqrt{N}$ for all outer-sphere bath modes, whereas the four intramolecular modes are harmonic with linear electronic-nuclear coupling. The results for $P(t)$ exhibit, in addition to the electronic coherence effects discussed above, oscillations on shorter timescales. These oscillations correspond to the vibrational periods of the four intramolecular modes and thus can be classified as vibrational coherence effects. The strong coupling strength between the intramolecular modes and the electronic states results in a weak temperature dependence of $P(t)$, which has also been found in previous studies of electron-transfer reactions in mixed-valence systems.^{52,54}

Although the outer-sphere bath modes are anharmonic for the model studied in Figure 5, this model can be exactly mapped to the standard harmonic bath spin–boson model because the intramolecular modes are harmonic. Figure 6 presents results for a model in which such a mapping is not possible because all intramolecular modes (and all bath modes) are intrinsically anharmonic. Since there is no fundamental restriction for selecting the anharmonic parameters of the intramolecular modes, we choose model parameters $A_j = B_j = D_j = E_j = F_j = G_j = 0.1$ for the intramolecular modes. All other parameters are kept the same as in Figure 5. It can be seen that, similar to what was found for the influence of the anharmonic bath, the anharmonicity in the intramolecular modes reduces the vibra-

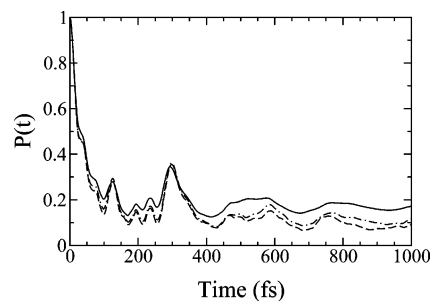


Figure 6. Time-dependent population of the donor electronic state for the generalized spin–boson model for which four intramolecular modes in Table 1 are included in addition to the outer-sphere bath. The anharmonic parameters in eq 2.10 are defined as $A_j = 0.2$ and $F_j = 0.2/\sqrt{N}$ for all outer-sphere bath modes and $A_j = B_j = D_j = E_j = F_j = G_j = 0.1$ for all intramolecular modes in addition to their harmonic potential and linear electronic-nuclear coupling. Three temperatures are shown: 300 (—), 100 (---), and 25 K (- - -).

tional coherence in $P(t)$. Furthermore, it also changes the potential energy surface significantly. As a result, the long time limit for the donor population, $P(t)$, is different from the value 0.5. The latter value was obtained for all models considered above, which could be mapped to a spin–boson model with fictitious harmonic bath. For the self-exchange ET reaction (with $E_1 = E_2 = 0$, corresponding to a symmetric spin–boson system) considered here, the spin–boson model with harmonic bath will give the limit $P(\infty) = 1/2$. The fact that the present model with anharmonic intramolecular modes does not give this limit is an indication that linear response is not valid and the model cannot be mapped to a fictitious harmonic bath.

Including anharmonic corrections for the strongly coupled intramolecular modes may thus have both thermodynamic and dynamic effects on electron-transfer reactions. This is illustrated in more detail in Figure 7. Panel (a) demonstrates how the transient dynamics and the long time value for the population changes if the anharmonicity of the intramolecular modes is increased systematically. The influence of the sign of the different anharmonic potential terms is studied in Figure 7b. In contrast to a purely harmonic spin–boson model, in which the sign of the linear coupling parameter c_j has no influence on the dynamics, this is not the case for models with anharmonic potentials, coupling terms, or both. Here, a different sign of the potential/coupling parameters may change the dynamics drastically due to the very different potential energy surface.

V. Concluding Remarks

In this paper, we have applied the multilayer multiconfiguration time-dependent Hartree (ML-MCTDH) theory to investigate electron-transfer reactions in the condensed phase employing models with anharmonic potential functions. We have studied both models that can, in principle, be mapped to a spin–boson model with a fictitious harmonic bath and models in which, due to anharmonicity in strongly coupled intramolecular degrees of freedom, such a mapping is not possible. The results show the influence of the anharmonicity on the ET dynamics. Depending on the specific model, it may result in more pronounced electronic coherence effects or a quenching of the electronic oscillation. For models that cannot be represented by a harmonic bath, the anharmonicity may, furthermore, alter the long-time limit of the electronic population significantly and thus influence the thermodynamics of the reaction.

The results presented in this paper demonstrate the capability of the ML-MCTDH method to accurately describe quantum dynamics in the condensed phase beyond the commonly

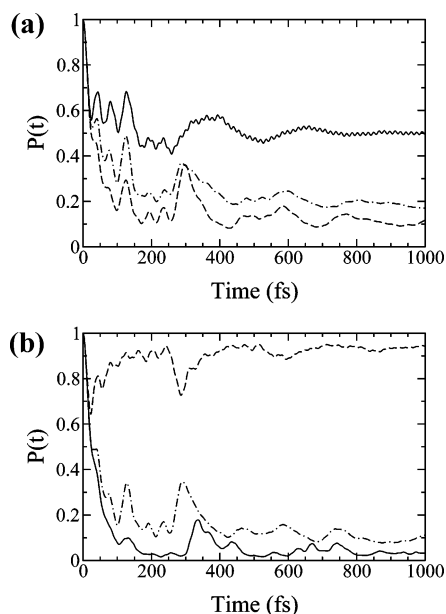


Figure 7. Time-dependent population of the donor electronic state for the generalized spin-boson model where intramolecular modes in Table 1 are included in addition to the outer-sphere bath. The anharmonic parameters in eq 2.10 are defined as $A_j = 0.2$ and $F_j = 0.2/\sqrt{N}$ for all outer-sphere bath modes, and for all intramolecular modes, the parameters are given, in addition to their harmonic potential and linear electronic-nuclear coupling as (a) $A_j = B_j = D_j = E_j = F_j = G_j = 0$ (—), $A_j = B_j = D_j = E_j = F_j = G_j = 0.05$ (---), $A_j = B_j = D_j = E_j = F_j = G_j = 0.1$ (- - -); (b) $A_j = E_j = F_j = G_j = 0.05$ and $B_j = D_j = -0.05$ (—), $A_j = B_j = E_j = F_j = G_j = 0.05$ and $D_j = -0.05$ (---), $A_j = B_j = D_j = F_j = G_j = 0.05$ and $E_j = -0.05$ (- - -). The temperature is 100 K.

employed harmonic bath model. This is of practical importance because many ET reactions involve large amplitude motion of low-frequency intramolecular modes that are strongly coupled to the electronic states, which cannot adequately be described in the harmonic approximation. Using more accurate potential functions, such as the models described in this paper, is crucial for capturing the quantum dynamics in these systems and providing correct interpretations of the time-resolved nonlinear spectroscopy. Finally, it should be noted that the ML-MCTDH theory can also be employed to study a broader class of models that include, in addition to anharmonic potentials, mode-mixing (Dushinski rotation)⁵⁵ of the different nuclear degrees of freedom. Work in this direction is in progress.

Acknowledgment. This work has been supported by the NSF-CAREER award CHE-0348956 (HW), the Deutsche Forschungsgemeinschaft (MT), and the Fonds der Chemischen Industrie (MT). The generous allocation of computing time by the National Energy Research Scientific Computing Center (NERSC) of the U.S. Department of Energy and the Leibniz Rechenzentrum, Munich, is gratefully acknowledged.

References and Notes

(1) Meyer, H.-D.; Manthe, U.; Cederbaum, L. S. *Chem. Phys. Lett.* **1990**, *165*, 73.

- (2) Manthe, U.; Meyer, H.-D.; Cederbaum, L. S. *J. Chem. Phys.* **1992**, *97*, 3199.
- (3) Beck, M. H.; Jäckle, A.; Worth, G. A.; Meyer, H.-D. *Phys. Rep.* **2000**, *324*, 1.
- (4) Meyer, H.-D.; Worth, G. A. *Theor. Chem. Acc.* **2003**, *109*, 251.
- (5) Wang, H.; Thoss, M. *J. Chem. Phys.* **2003**, *119*, 1289.
- (6) Raab, A.; Worth, G.; Meyer, H.-D.; Cederbaum, L. *J. Chem. Phys.* **1999**, *110*, 936.
- (7) Huarte-Larranaga, F.; Manthe, U. *J. Chem. Phys.* **2000**, *113*, 5115.
- (8) Mahapatra, S.; Worth, G. A.; Meyer, H. D.; Cederbaum, L. S.; Köppel, H. *J. Phys. Chem. A* **2001**, *105*, 5567–5576.
- (9) Cattarius, C.; Worth, G. A.; Meyer, H.-D.; Cederbaum, L. S. *J. Chem. Phys.* **2001**, *115*, 2088–2100.
- (10) Nauendorf, H.; Worth, G.; Meyer, H.-D.; Kühn, O. *J. Phys. Chem.* **2002**, *106*, 719–724.
- (11) Coutinho-Neto, M. D.; Viel, A.; Manthe, U. *J. Chem. Phys.* **2004**, *121*, 9207–9210.
- (12) Wu, T.; Werner, H.-J.; Manthe, U. *Science* **2004**, *306*, 2227.
- (13) Worth, G. A.; Meyer, H.-D.; Cederbaum, L. S. *J. Chem. Phys.* **1998**, *109*, 3518.
- (14) Wang, H. *J. Chem. Phys.* **2000**, *113*, 9948.
- (15) Egorova, D.; Thoss, M.; Domcke, W.; Wang, H. *J. Chem. Phys.* **2003**, *119*, 2761.
- (16) Nest, M.; Meyer, H.-D. *J. Chem. Phys.* **2003**, *119*, 24.
- (17) Burghardt, I.; Nest, M.; Worth, G. *J. Chem. Phys.* **2003**, *119*, 5364.
- (18) Leggett, A. J.; Chakravarty, S.; Dorsey, A. T.; Fisher, M. P. A.; Garg, A.; Zwerger, W. *Rev. Mod. Phys.* **1987**, *59*, 1.
- (19) Weiss, U. *Quantum Dissipative Systems*, 2nd ed.; World Scientific: Singapore, 1999.
- (20) Marcus, R. A.; Sutin, N. *Biochim. Biophys. Acta* **1985**, *811*, 265.
- (21) Wang, H.; Thoss, M.; Miller, W. H. *J. Chem. Phys.* **2001**, *115*, 2979.
- (22) Wang, H.; Thoss, M. *Isr. J. Chem.* **2002**, *42*, 167.
- (23) Coalson, R. D. *J. Chem. Phys.* **1986**, *86*, 6823.
- (24) Mak, C. H.; Chandler, D. *Phys. Rev. A: At., Mol., Opt. Phys.* **1991**, *44*, 2352.
- (25) Egger, R.; Weiss, U. *Z. Phys. B* **1992**, *89*, 97.
- (26) Egger, R.; Mak, C. H. *Phys. Rev. B: Condens. Matter Mater. Phys.* **1994**, *50*, 15210.
- (27) Makri, N.; Makarov, D. E. *J. Chem. Phys.* **1995**, *102*, 4600.
- (28) Stockburger, J.; Mak, C. H. *Phys. Rev. Lett.* **1998**, *80*, 2657.
- (29) Mühlbacher, L.; Egger, R. *J. Chem. Phys.* **2003**, *118*, 179.
- (30) Thorwart, M.; Reimann, P.; Hänggi, P. *Phys. Rev. E: Stat. Phys., Plasmas, Fluids, Relat. Interdiscip. Top.* **2000**, *62*, 5808.
- (31) Feynman, R. P.; Vernon, A. R. *Ann. Phys.* **1963**, *24*, 118.
- (32) Wang, H.; Thoss, M. *Chem. Phys. Lett.* **2004**, *389*, 43.
- (33) Thoss, M.; Kondov, I.; Wang, H. *Chem. Phys.* **2004**, *304*, 169.
- (34) Thoss, M.; Domcke, W.; Wang, H. *Chem. Phys.* **2004**, *296*, 217.
- (35) Jortner, J.; Bixon, M. *Electron Transfer: From Isolated Molecules to Biomolecules, Dynamics and Spectroscopy. Adv. Chem. Phys.*; Wiley: New York, 1999; Vol. 106–107.
- (36) Georgievskii, Y.; Hsu, C.-P.; Marcus, R. A. *J. Chem. Phys.* **1999**, *110*, 5307.
- (37) Makri, N. *J. Phys. Chem. B* **1999**, *103*, 2823.
- (38) Sondergaard, N.; Ulstrup, J.; Jortner, J. *Chem. Phys.* **1976**, *17*, 417.
- (39) Islampour, R.; Lin, S. *Chem. Phys. Lett.* **1991**, *179*, 147.
- (40) Tang, J. *Chem. Phys.* **1993**, *179*, 105.
- (41) Kalyanaraman, C.; Evans, D. J. *Chem. Phys.* **2001**, *115*, 7076.
- (42) Lockwood, D. M.; Ratner, M. A.; Kosloff, R. *J. Chem. Phys.* **2002**, *117*, 10125.
- (43) Brisker, D.; Peskin, U. *J. Chem. Phys.* **2006**, *1125*, 111103.
- (44) Ilk, G.; Makri, N. *J. Chem. Phys.* **1994**, *101*, 6708.
- (45) Makri, N. *J. Chem. Phys.* **1999**, *111*, 6164.
- (46) Evans, D. G. *J. Chem. Phys.* **2000**, *113*, 3282.
- (47) Wang, H.; Thoss, M. *Chem. Phys.* **2004**, *304*, 121.
- (48) Suárez, A.; Silbey, R. *J. Chem. Phys.* **1991**, *95*, 9115.
- (49) Makri, N. *J. Phys. Chem. A* **1998**, *102*, 4414.
- (50) Thoss, M.; Wang, H. *Chem. Phys.* **2006**, *322*, 210.
- (51) Kondov, I.; Thoss, M.; Wang, H. *J. Phys. Chem. A* **2006**, *110*, 1364.
- (52) Wang, H.; Thoss, M. *J. Phys. Chem. A* **2003**, *107*, 2126.
- (53) Wang, H.; Thoss, M. *J. Chem. Phys.* **2006**, *124*, 034114.
- (54) Thoss, M.; Wang, H. *Chem. Phys. Lett.* **2002**, *358*, 298.
- (55) Dushinski, F. *Acta Physicochim. URSS* **1937**, *7*, 551.